

Impact of a New Radiation Package in the ECMWF Integrated Forecast System

J.-J. Morcrette

ECMWF

Shinfield Park, Reading, UK

Email: Jean-Jacques.Morcrette@ecmwf.int

ABSTRACT

The Monte-Carlo Independent Column Approximation (McICA) was recently introduced by Barker et al. (2003) and Pincus et al. (2003) as a flexible way to ensure an unbiased if noisy description of the radiative fields over appropriate time and space scales in a large-scale model of the atmosphere. McICA is here introduced as part of a new radiation transfer package (McRad) for the ECMWF forecast model and tested in both low-resolution seasonal simulations and high-resolution ten-day forecasts.

The impact of McRad on year-long simulations with a low-resolution ($T_L 159L91$) version of the model and of ten-day forecasts at higher resolution is explored, with comparisons made against observations and the operational model configuration. In long simulations, McRad has a marked effect in reducing some systematic errors in the position of tropical convection, due to change in the overall distribution of diabatic heating over the vertical, inducing a geographical redistribution of the centres of convection. At high resolution, with respect to forecasts carried out with the standard radiation schemes, McRad has a small (generally positive) on objective scores of the geopotential and a larger impact on temperatures, with a warming of the lower troposphere and a cooling of the upper troposphere and lower stratosphere.

Finally, the flexibility of McICA approach in dealing with cloud overlap and cloud inhomogeneity is illustrated in an additional series of seasonal simulations with the cloud generator and the new package of radiation schemes handling either a generalized overlapping inhomogeneous clouds or the previously assumed maximum-random overlapping plane-parallel clouds.

1 Introduction

At the grid-scale of a large-scale atmospheric model (LSAM), domain-averaged radiative fluxes in clouds with substantial horizontal and vertical variability can in principle be determined quite accurately using the plane-parallel independent column approximation (ICA) by averaging the flux computed for each class of cloud in turn (Cahalan et al., 1994; Barker et al., 1999). This approach neglects true three-dimensional effects, but those are generally minor (Barker et al., 2003a). Unfortunately, such an ICA-based method is too computationally expensive for dealing with radiation transfer (RT) in a LSAM. Various approximations have been introduced over the years to compute domain-averaged radiative fluxes for internally variable clouds, all invoking assumptions about the nature of the horizontal variability (e.g., Stephens, 1988; Oreopoulos and Barker, 1999; Cairns et al., 2000) or how cloud layers are linked over the vertical (Geleyn and Hollingsworth, 1979; Morcrette and Jakob, 2002; Li, 2002). Regardless of what assumptions are made about these unresolved structures, estimates of radiative heating should theoretically become increasingly unbiased at increasingly large spatial and temporal scales. However, this is generally not the case, and climate simulations have been shown to be very sensitive to seemingly small, but systematic, alterations to cloud optical properties (e.g., Senior, 1999).

Recently, Barker et al. (2003b) and Pincus et al. (2003) introduced a new method for computing broadband

radiative fluxes in LSAMs yielding unbiased radiative fluxes over an ensemble average of one-dimensional RT simulations. It is referred to as the Monte-Carlo Independent Column Approximation (McICA). The most attractive features of McICA are two-fold: first, it extricates the description of the sub-grid scale cloud structure from the radiative transfer algorithm through a cloud generator that provides the cloud parameters for the radiation schemes by sampling the cloud information randomly from the cloud fraction and water profiles provided by the LSAM; second, its radiative fluxes, unbiased w.r.t. ICA, are consistent with assumptions made about the unresolved structure in other parts of the model. In practice, this sub-grid scale cloud structure is related either to the overlapping of the cloud layers in the vertical and/or to the horizontal variability of the cloud characteristics. Whether on the vertical or on the horizontal, the cloud characteristics referred to above correspond to input parameters in a traditional radiation transfer scheme, namely the distribution of condensed water in various phases, that of the particle effective dimension, which together with the distribution of intervening gases should define the radiation exchange on the vertical within a grid of the LSAM. As ICA, McICA does not account for true 3-dimensional transfer effects, but those can generally be neglected. As an illustration of the method, the McICA approach was recently tested on fields produced every 3 hours over a day by a cloud-resolving-model (CRM) embedded in a LSAM (Räisänen et al., 2003).

In the following, we present preliminary results of the impact of the McICA approach to radiation transfer within the forecast model of the European Centre for Medium-Range Weather Forecasts (ECMWF). The implementation of McICA in a new radiation package for the ECMWF model (hereafter referred to as McRad) is briefly described in section 2, with more details concerning the cloud generator and the two radiation schemes.

Results obtained in seasonal simulations with the $T_L 159$ L91 version of the ECMWF model, with specified sea surface temperature, are discussed in section 3. Impact of McRad in ten-day forecasts at $T_L 319$ L91 resolution is described in section 4.

Then, in section 5, we illustrate the flexibility inherent in the McICA approach and compares results assuming maximum-random cloud overlapping of homogeneous plane-parallel clouds with results assuming a generalized overlap of inhomogeneous cloud layers. A summary and conclusions are presented in section 6.

2 The method

2.1 Theoretical background

The McICA approach is an approximation to the full Independent Column Approximation (ICA). As discussed by Barker et al. (2003b) and Pincus et al. (2003), for the full ICA, the average monochromatic radiative flux, over a domain sub-divided in N columns, in which each layer can only have a cloud fraction of 0 or 1, is

$$\langle F \rangle = \frac{1}{N} \sum_{n=1}^N F_n \quad (1)$$

In sub-column n , using a radiation parametrisation (plane-parallel, and considering a homogeneous cloud water distribution in all overcast layers) with a correlated k-distribution (CKD) approach to deal with absorption, the total flux F_n is

$$F_n = \sum_{k=1}^K c_k F_{n,k} \quad (2)$$

Combining (1) and (2) gives

$$\langle F \rangle = \frac{1}{N} \sum_{n=1}^N \sum_{k=1}^K c_k F_{n,k} \quad (3)$$

With the version of the ECMWF model used for this study, the radiation fluxes are computed using the Rapid Radiation Transfer Models (RRTM), both in the longwave and shortwave parts of the spectrum. The $RRTM_{LW}$ and $RRTM_{SW}$ radiation codes have a K respectively of 140 and 112 (number of g-points in the cumulative probability space directly derived from the correlated k-distribution), so a code explicitly integrating the double sum in (3) would be far too expensive for GCM applications.

The McICA solution to this problem is to approximate (3) as

$$\langle F \rangle_M = \sum_{k=1}^K F_{n_k,k} \quad (4)$$

where $F_{n_k,k}$ is the monochromatic radiative flux for a single randomly selected sub-column η_k .

From this definition, the McICA solution (4) equals the ICA solution only when all N sub-columns are identical or $N = 1$. As discussed in Räisänen and Barker (2004), McICA's incomplete pairing of sub-columns and spectral intervals ensures that its solution will contain random, but unbiased, errors.

McICA can in principle be used within any radiation transfer scheme provided a cloud generator is used to define how the cloud information is distributed over each spectral element in the radiation spectrum.

The application of the McICA approach involves using a cloud generator together with slightly modified but otherwise standard radiation schemes. A description of the radiation transfer schemes and of the cloud generator used in this study is given below.

2.2 Practical implementation of McICA in the ECMWF model

Table 1 summarized the main features of the radiation package used in this study. The ECMWF version of $RRTM_{LW}$ (Mlawer et al., 1997, Morcrette et al., 2001) describes the longwave spectrum with 16 spectral intervals, corresponding to a total of 140 g-points. $RRTM_{SW}$ (Mlawer and Clough, 1997) describes the shortwave spectrum with 14 spectral intervals, corresponding to a total of 112 g-points. Each spectral interval might have a different number of g-points, depending how much the absorption coefficient varies within the spectral interval, but also how much the spectral interval contributes overall to the total flux, and this over the whole depth of the atmosphere represented by the atmospheric model. For each of these g-points, an essentially monochromatic type radiation transfer is carried out using a two-stream method using an approximate provision for the LW scattering and using a Delta two-stream method with scattering in the shortwave. For its initial testing in the ECMWF model (in non McICA mode), cloud fractional cover in $RRTM_{SW}$ was treated as discussed in Briegleb (1992) and Liou (1992). For liquid water clouds, the effective droplet radius is diagnosed following Martin et al. (1994); the effective ice particle size is diagnosed following a modification of Ou and Liou (1995) in the reference scheme, and following Sun (2001) in the McRad scheme.

The McICA versions of $RRTM_{LW}$ and $RRTM_{SW}$ differ from the above versions in two respects: i/ Avoiding any explicit reference to cloud fraction greatly simplifies the part of the algorithms devoted to the vertical integration, which now deals simply with optical thicknesses. For a given g-point, a cloud when present fully occupies a model layer. Therefore any cloudy calculation only involves modifying the optical parameters (τ , ω , g). ii/ This allows to get rid of the 0.7 factor multiplying the cloud optical thickness, which had been introduced in 1997 (Cahalan et al., 1994; Tiedke, 1996) in the ECMWF Integrated Forecasting System (IFS) to account approximately for the effect of cloud inhomogeneities at the sub-grid level.

As stated in the Introduction and Section 2a, the McICA representation of cloud-radiation interactions requires the cloud information to be distributed by a cloud generator over the vertical with the constraint that the total cloudiness and cloud water loading for a grid-point is conserved.

The purpose of the cloud generator is, starting from a cloud profile (cloud fraction and cloud water content) provided by a traditional cloud scheme (e.g., Tiedtke, 1993), to distribute randomly the cloud information (in terms of presence (1) or absence (0)) into each of the layers covered by the original cloud profile. This distribution is done N times (McICA with N going to infinity would be equal to ICA) with the constraint that a summation over the N profiles would recreate the original vertical distribution of partial cloudiness. In the ECMWF model, for each radiation time-step (every one hour of model time) and each grid-point, the cloud generator is used twice, to produce two cloud distributions relevant, respectively, to the 140 g-points of the LW- and 112 g-points of SW radiation schemes. We use the cloud generator of Räisänen et al. (2004), which vertically can distribute either the cloud cover according to a maximum-random overlap assumption or both the cloud cover and cloud water assuming a generalized overlap (Hogan and Illingworth, 2000, 2003).

Most of the results presented hereafter corresponds to a generalized overlap with decorrelation lengths of 2 km for cloud cover and 1 km for cloud water, and a normalized standard deviation of the cloud condensate of 1. Only in section 5, will results corresponding to a generalized overlap with different decorrelation lengths, or to maximum-random overlap of the cloud layers be discussed.

Clouds when present occupy the full horizontal extent of the layer, and the vertical distribution of such clouds (of 0 or 1 cloud cover) is defined independently for each of the 140 (112) g-points of the longwave (shortwave) scheme by the cloud generator, with the constraint that the total cloudiness and cloud water loading for a grid-point is conserved when N tends to infinity.

In all comparisons discussed hereafter, the non McICA model (CY30R2 or CY31R2) uses the ECMWF 6 spectral interval version of the shortwave radiation code of Fouquart and Bonnel (1980), with a slightly different set of cloud optical properties. Previous studies have shown that cloud optical properties had a relatively small impact on the model simulations.

3 Results for seasonal simulations at $T_L 159L91$ with specified SSTs

Sets of seasonal simulations have been carried over the 13-month period between August 2000 and September 2001, with the cycle 30R2 of the ECMWF IFS system library. Each set includes 3 simulations starting 24-hours apart, with output parameters averaged over the September'00-August'01 period presented as maps in Figs. 1 to 7. Global mean values for an extended list of parameters are given in Table 1, averaged over the year, and over the DJF and JJA three-month periods.

3.1 Radiative fields at the top of the atmosphere

Figures 1 to 4 respectively present comparisons of the annual mean outgoing longwave radiation at TOA (OLR: Fig.1), absorbed shortwave radiation (ASW: Fig.2), longwave cloud forcing (LWCF: Fig.3) and shortwave cloud forcing (SWCF: Fig.4) with corresponding parameters from CERES observations. The McRad package improves the behaviour of the model in a number of aspects: first and foremost, a change in the balance between longwave and shortwave radiation heating leads to a noticeable shift in the location of the tropical cloudiness. This is a feature of McRad, as preliminary tests using $RRTM_{SW}$ (without the McICA approach) instead of the operational shortwave radiation code, or different set of cloud optical properties, changed somewhat the overall radiation budget at the top of the atmosphere, but without affecting the negative bias linked to a too small cloudiness over tropical South America, Africa and the West Pacific.

The McRad package improves markedly on the TOA radiation biases over these areas. Differences with CERES observations are improved with the new model, with a reduction of the global annual mean bias from -8 to -3.2 W m^{-2} for OLR (Fig.1), from -10 to -5.8 W m^{-2} for ASW (Fig.2), from -9.6 to -4 W m^{-2} for LWCF (Fig.3), and from -5.2 to -0.2 W m^{-2} for SWCF. This is clearly linked to a change in the position of the convective activity. The decrease in the continental negative bias in OLR over tropical South America, Africa and the West Pacific, and the decrease in the oceanic negative bias in ASW over most oceans shows that some spurious cloudiness occurring over oceans in the reference simulation has moved to a more proper location over the continents with McRad. The same explanation is valid for the improvement in tropical longwave and shortwave cloud forcing (LWCF and SWCF). For LWCF at higher latitudes, improvement can also be related to the change in cloud optical properties, particularly to the diagnostic of effective size particle from temperature and local ice water content in McRad, compared to a diagnostic from temperature only in the CY30R2 operational radiation code. Table 2 confirms that these improvements happen over the whole year, with a general improvement on the TOA radiative parameters also appearing for winter (DJF) and summer (JJA) conditions.

3.2 Hydrological budget

As seen also in Table 2, the overall climate of the model is also improved in terms of the global water vapour (TCWV: total column water vapour) and cloud water distribution (TCLW: total column liquid water), and level of total precipitation (TP, compared in Table 2 to GPCP and SSM/I estimates). The only degradation is seen in surface SW radiation, which shows the annual mean difference to the Da Silva climatology (over oceans only) roughly doubled. This is directly partly linked to slightly more transparent clouds induced by the McICA approach, but mostly to the transfer of convective cloudiness from tropical oceanic to tropical continental areas.

However, despite the increase in surface SW radiation over the tropical oceans, it is expected that for the ECMWF model including an interactive ocean, the better geographical distribution of surface fluxes produced by McRad will be beneficial to the forecasts of ocean surface temperature.

Figure 5 presents the total precipitation and its comparison with GPCP observations. The improvements are less marked than for radiation fields. However a reduction of the deficit of precipitation over South America and Africa and a slight reduction of the overestimation of precipitation over the Pacific, Atlantic and Indian oceans are present, confirmed by the better global results, on an annual or seasonal basis, seen for total precipitation in Table 2, whether compared to GPCP or SSM/I.

3.3 Temperature, humidity and wind errors

Figures 6 and 7 respectively the zonal mean differences of temperature and humidity (Fig.6) and zonal wind and vertical velocity (Fig.7) averaged over the year. The McRad package improves on the temperature differences (Fig.6 top) to ERA40 analyses, showing an overall warming of the troposphere, and a cooling of the stratosphere. This translates into a slight improvement in the zonal mean humidity w.r.t. ERA40 (Fig.6 bottom). The impact on zonal mean zonal wind is somewhat smaller but generally positive. Impact on vertical velocity is mainly seen in the tropical area with a slight decrease in both the negative and positive difference to ERA40 between 30°N and 30°S .

4 Results for 10-day forecasts at $T_L319L91$

Results are presented for a set of 108 10-day forecasts, with the cycle 31R2 of the IFS library, at $T_L319L91$, started every 24 hours from the operational analyses, between 20060212 12UTC and 20060531 12UTC. The impact of McRad is minimum on anomaly correlation and root mean square error of geopotential, as illustrated in Fig. 8 for the geopotential at 500 hPa over the Northern and Southern hemispheres, and over the European area. A similar signal is seen over the whole vertical. The root mean square and mean error in temperature over the Northern and Southern hemispheres, and the tropics (20°N - 20°S) are presented in Figs. 9, 10 and 11 for the 850, 200 and 50 hPa, respectively. As already seen in long simulations, the main impact of McRad is a warming of the lower tropospheric layers and a cooling of the upper troposphere and lower stratosphere. Overall, McRad improves on the temperature objective scores. Where on the vertical the transition between a lower down warming and a higher up cooling occurs depends on the season, between 500 and 300 hPa in the summer hemisphere, between 700 and 500 hPa in the winter hemisphere, around 300 hPa in the tropics. This structure of the temperature impact of McRad is a feature appearing whatever the model horizontal resolution. Resulting from a better temperature structure, the wind also displays some improvement. Figures 12 and 13 present the absolute correlation and the root mean square error of the wind at 850 hPa (Fig.12) and 200 hPa (Fig.13) over the Northern and Southern hemispheres, and the tropics. The wind produced by the model with McRad is very slightly better over the Northern and Southern hemispheres, with the larger improvement in the tropics, particularly at 200 hPa.

5 About overlap and inhomogeneous clouds

As already indicated in the Introduction, the use of a cloud generator external to the LW and SW radiation schemes to deal with the vertical overlap of clouds layers and potential inhomogeneity in the horizontal distribution of cloud water content makes easy the testing of various configurations. Sets of seasonal simulations were carried out in the same conditions as those in section 3, with the McRad cycle 31R1 model configuration and different assumptions for the cloud vertical overlap and horizontal distribution of cloud water. As can be seen from Fig.14, the impact of various decorrelation lengths for cloud cover (DLCC) or cloud water (DLCW), or switching to a maximum-random cloud overlap with provision for inhomogeneous cloud water distribution is much smaller than the impact of introducing the new radiation package. As can be seen from Table 3, each of these configurations is slightly different in terms of impact on radiation and other physical fields, and the configuration chosen for more extensive experimentation is the one which gives the best overall comparisons to observations.

6 Timing issues

The introduction of McRad in the ECMWF IFS introduces a sizeable increase in the computer time required for carrying out a given forecast. It is again to be stressed that this increase is *not* related to the McICA approach, as the McICA versions of $RRTM_{LW}$ and $RRTM_{SW}$ are slightly faster than the original versions as they are not dealing with fractional cloudiness, but just optical thicknesses, whether originating from clear-sky absorbers and aerosols, or the same plus cloud optical thickness. The increase is mainly linked to the use of $RRTM_{SW}$ with its 112 g-point radiative transfer computations compared with computations over the 6 spectral intervals of the operational SW scheme (Fouquart and Bonnel, 1980; Morcrette, 2002). Table 4 presents for the various model configurations used at ECMWF an overview of the timing with and without McRad. Given this increase, it is expected that the ECMWF operational configurations will change from D799R399 to D799R319

for the high-resolution forecast, whereas Ensemble Prediction System and climate-type simulations will keep the same configuration (respectively, D399R159 and D159R63).

7 Summary and conclusions

The Monte-Carlo Independent Column Approximation allows the separation of the definition of the cloud from its impact in the radiation transfer. As such, it simplifies the radiation transfer schemes by suppressing all references to partial cloud cover, the subsequent separate calculations for clear-sky and cloudy parts of the layers, and the inherent complexity of the vertical integration accounting for the overlapping of these clear and cloudy quantitites (reflectances/transmittances or fluxes). The cloud generator used here (Räisänen and Barker, 2004) being independent from the radiation transfer can now handle any overlap situation, and is used here with either a maximum-random of homogeneous cloud layers or a definition of the overlap of cloud layers through decorrelation length (Hogan and Illingworth, 2000).

The Monte-Carlo Independent Column Approximation was implemented in the ECMWF forecast system, and the impact of the so-called McRad radiation package was studied in seasonal simulations and 10-day forecasts w.r.t. equivalent simulations and forecasts carried out with the operational radiation schemes. In both configurations, the McRad package was shown to improve on the operational radiation scheme.

The McRad is more expensive than the operational radiation package mainly due to the use of the more recent, more spectrally detailed, but also better validated $RRTM_{SW}$ shortwave scheme (as part of the BroadBand Heating Rate Profile Value-Added Project (BBHRP-VAP) effort within the ARM community, Mlawer et al., 2007). Despite its larger computational cost, it is felt that this new radiation package represents the way forward in radiative parametrisations for LSAMs for a number of reasons:

- 1/ Its flexibility in handling various overlap assumptions (in particular, it could easily handle vertical overlap information derived from active cloud remote sensing instruments (lidar, radar).
- 2/ It provides a framework for coupling the radiation transfer calculations with cloud information derived from pdf-based cloud schemes (Tompkins, 2002).
- 3/ Within the framework of LSAMs, the McICA approach would allow the same overlap assumption to be used for radiation transfer and precipitation/evaporation processes, a problem up-to-now solved either only approximately (Jakob and Klein, 2000) or through additional calculations (Jakob and Klein, 1999).
- 4/ The McICA approach can easily (if expensively) be transformed back to the ICA approach, which apart from its neglect of three-dimensional effects (but thought to be of secondary importance) provides a benchmark for radiative transfer calculations.

Acknowledgements

Drs E. Mlawer, M. Iacono, J. Delamere, and A. Clough (AER, Inc.) provided both the original RRTM long-wave and shortwave radiation codes, that were adapted to the ECMWF model and modified to include the McICA approximation to deal with cloudiness. Drs H. Barker and R. Pincus convinced the author to initiate this work and maintained the pressure till McICA was properly tested in the ECMWF IFS. Dr P. Räisänen wrote the cloud generator, and Dr J. Cole answered a number of queries on the cloud generator. At ECMWF, Drs D. Salmond and J. Hague helped in the debugging and optimization of the code. Finally Drs M. Miller, A. Beljaars and A. Tompkins are thanked for their comments at different stages of this work.

REFERENCES

- Barker, H.W., G.L. Stephens, and Q. Fu, 1999: The sensitivity of domain-averaged solar fluxes to assumptions about cloud geometry. *Quart. J. Roy. Meteor. Soc.*, **125**, 2127-2152.
- Barker, H.W., R. Pincus, and J.-J. Morcrette, 2003b: The Monte-Carlo Independent Column Approximation: Application within large-scale models. *Proceedings GCSS/ARM Workshop on the Representation of Cloud Systems in Large-Scale Models*, May 2002, Kananaskis, AB, Canada, 10 pp.
<http://www.met.utah.edu/skrueger/gcss-2002/Extended-Abstracts.pdf>
- Barker, H.W., G.L. Stephens, P.T. Partain, and J.-J. Morcrette among 29 others, 2003a: Assessing 1D atmospheric solar radiative transfer models: Interpretation and handling of unresolved clouds. *J. Climate*, **16**, 2676-2699.
- Briegleb, B.P., 1992: Delta-Eddington approximation for solar radiation in the NCAR Community Climate Model. *J. Geophys. Res.*, **97**, 7603-7612.
- Cahalan, R.F., Ridgway, W., W.J. Wiscombe, S. Gollmer, and Harshvardhan, 1994: Independent pixel and Monte Carlo estimates of stratocumulus albedo. *J. Atmos. Sci.*, **51**, 3776-3790.
- Cairns, B., A.A. Lacis, and B.E. Carlson, 2000: Absorption within inhomogeneous clouds and its parameterization in general circulation models. *J. Atmos. Sci.*, **57**, 700-714.
- Ebert, E.E., and J.A. Curry, 1992: A parametrization of ice cloud optical properties for climate models. *J. Geophys. Res.*, **97D**, 3831-3836.
- Fouquart, Y., 1987: *Radiative transfer in climate models*. NATO Advanced Study Institute on Physically-Based Modelling and Simulation of Climate and Climatic Changes. Erice, Sicily, 11-23 May 1986. M.E. Schlesinger, Ed., Kluwer Academic Publishers, 223-284.
- Fouquart, Y., and B. Bonnel, 1980: Computations of solar heating of the earth's atmosphere: a new parameterization. *Beitr. Phys. Atmosph.*, **53**, 35-62.
- Fu, Q., 1996: An accurate parameterization of the solar radiative properties of cirrus clouds for climate studies. *J. Climate*, **9**, 2058-2082.
- Fu, Q., P. Yang, and W.B. Sun, 1998: An accurate parameterization of the infrared radiative properties of cirrus clouds of climate models. *J. Climate*, **11**, 2223-2237.
- Geleyn, J.-F., and A. Hollingsworth, 1979: An economical analytical method for the computation of the interaction between scattering and line absorption of radiation. *Beitr. Phys. Atmosph.*, **52**, 1-16.
- Hogan, R.J., and A.J. Illingworth, 2000: Deriving cloud overlap statistics from radar. *Quart. J. Roy. Meteor. Soc.*, **126**, 2903-2909.
- Hogan, R.J. and A.J. Illingworth, 2003: Parameterizing ice cloud inhomogeneity and the overlap of inhomogeneities using cloud radar data. *J. Atmos. Sci.*, **60**, 756-767.
- Jakob, C., and S.A. Klein, 1999: The role of vertically varying cloud fraction in the parametrization of microphysical processes in the ECMWF model. *Quart. J. Roy. Meteor. Soc.*, **125**, 941-965.
- Jakob, C., and S.A. Klein, 2000: A parametrization of the effects of cloud and precipitation overlap for use in general circulation models. *Quart. J. Roy. Meteor. Soc.*, **126**, 2525-2544.
- Li, J., 2002: Accounting for unresolved clouds in a 1D infrared radiative transfer code. Part I: Solution for radiative transfer , including cloud scattering and overlap. *J. Atmos. Sci.*, **59**, 3302-3320.

- Lindner, T.H., and J. Li, 2000: Parameterization of the optical properties for water clouds in the infrared. *J. Climate*, **13**, 1797-1805.
- Liou, K.-N., 1992: *Radiation and Cloud Processes*, Oxford University Press, Oxford, 487 pp.
- Martin, G.M., D.W. Johnson, and A. Spice, 1994: The measurement and parameterization of effective radius of droplets in warm stratocumulus. *J. Atmos. Sci.*, **51**, 1823-1842.
- Mlawer, E.J., and S.A. Clough, 1997: Shortwave and longwave enhancements in the Rapid Radiative Transfer Model, in Proceedings of the 7th Atmospheric Radiation Measurement (ARM) Science Team Meeting, U.S. Department of Energy, CONF-9603149.
<http://www.arm.gov/publications/proceedings/conf07/title.stm/mlaw-97.pdf>
- Mlawer, E.J., S.J. Taubman, P.D. Brown, M.J. Iacono, and S.A. Clough, 1997: Radiative transfer for inhomogeneous atmospheres: RRTM, a validated correlated-k model for the longwave. *J. Geophys. Res.*, **102D**, 16,663-16,682.
- Mlawer et 24 co-authors. (2007):
<http://www.arm.gov/publications/proceedings/conf17/display.php?id=MjU2>
<http://engineering.arm.gov/shippert/BBHRP/index.html>
- Morcrette, J.-J., 2002: Assessment of the ECMWF model cloudiness and surface radiation fields at the ARM-SGP site. *Mon. Wea. Rev.*, **130**, 257-277.
- Morcrette, J.-J., and C. Jakob, 2000: The response of the ECMWF model to changes in cloud overlap assumption. *Mon. Wea. Rev.*, **128**, 1707-1732.
- Morcrette, J.-J., E.J. Mlawer, M.J. Iacono, and S.A. Clough, 2001: Impact of the radiation transfer scheme RRTM in the ECMWF forecasting system. *ECMWF Newsletter*, **91**, 2-9.
- Oreopoulos, L. and H. W. Barker, 1999: Accounting for subgrid-scale cloud variability in a multi-layer 1D solar radiative transfer algorithm. *Quart. J. Roy. Meteor. Soc.*, **125**, 301-330.
- Ou, S.C., and K.-N. Liou, 1995: Ice microphysics and climatic temperature feedback. *Atmosph. Research*, **35**, 127-138.
- Pincus, R., H.W. Barker, and J.-J. Morcrette, 2003: A fast, flexible, approximate technique for computing radiative transfer in inhomogeneous clouds. *J. Geophys. Res.*, **108D**, 4376, doi:10.1029/2002JD003322.
- Räisänen, P., and H.W. Barker, 2004: Evaluation and optimization of sampling errors for the Monte Carlo Independent Column Approximation. *Quart. J. Roy. Meteor. Soc.*, **130**, 2069-2085.
- Räisänen, P., H.W. Barker, M. Khairoutdinov, J. Li, and D.A. Randall, 2004: Stochastic generation of subgrid-scale cloudy columns for large-scale models. *Quart. J. Roy. Meteor. Soc.*, **130**, 2047-2067.
- Räisänen, P., G.A. Isaac, H.W. Barker, and I. Gultepe, 2003b: Solar radiative transfer for stratiform clouds with horizontal variations in liquid water path and droplet effective radius. *Quart. J. Roy. Meteor. Soc.*, **129**, 2135-2149.
- Senior, C.A., 1999: Comparison of mechanisms of cloud-climate feedbacks in GCMs. *J. Climate*, **12**, 1480-1489.
- Slingo, A., 1989: A GCM parameterization for the shortwave radiative properties of water clouds. *J. Atmos. Sci.*, **46**, 1419-1427.
- Smith, E. A., and Lei Shi, 1992: Surface forcing of the infrared cooling profile over the Tibetan plateau. Part I: Influence of relative longwave radiative heating at high altitude. *J. Atmos. Sci.*, **49**, 805-822.

- Stephens, G.L., 1988: Radiative transfer through arbitrarily shaped optical media: Part I: A general method of solution. *J. Atmos. Sci.*, **45**, 1818-1836.
- Sun, Z., 2001: Reply to comments by G.M. McFarquhar on "Parametrization of effective sizes of cirrus-cloud particles and its verification against observations". *Quart. J. Roy. Meteor. Soc.*, **127A**, 267-271.
- Tiedtke, M., 1993: Representation of clouds in large-scale models. *Mon. Wea. Rev.*, **121**, 3040-3061.
- Tiedtke, M., 1996: An extension of cloud-radiation parameterization in the ECMWF model: The representation of sub-grid scale variations of optical depth. *Mon. Wea. Rev.*, **124**, 745-750.
- Tompkins, A.M., 2002: A prognostic parameterization for the sub-grid scale variability of water vapor and clouds in large-scale models and its use to diagnose cloud cover. *J. Atmos. Sci.*, **59**, 1917-1942.

Table 1: Characteristics of the longwave and shortwave radiation schemes

	$RRTM_{LW}$	$RRTM_{SW}$
Solution of RT Equation	two-stream method	two-stream method
Number of spectral intervals	16 (140 g-points)	14 (112 g-points)
Absorbers	$H_2O, CO_2, O_3, CH_4, N_2O, CFC11, CFC12, \text{aerosols}$	$H_2O, CO_2, O_3, CH_4, N_2O, CFC11, CFC12, \text{aerosols}$
Spectroscopic database	HITRAN, 1996	HITRAN, 1996
Absorption coefficients	from LBLRTM line-by-line model	from LBLRTM line-by-line model
Cloud handling	true cloud fraction	true cloud fraction
Cloud optical properties method	16-band spectral emissivity	14-band τ, g, ω
Data: ice clouds	Ebert & Curry, 1992 Fu et al., 1998	Ebert & Curry, 1992 Fu, 1996
water clouds	Smith & Shi, 1992 Lindner & Li, 2000	Fouquart, 1987 Slingo, 1989
Cloud overlap assumption set up in cloud generator	maximum-random or generalized	maximum-random or generalized
Reference	Mlawer et al., 1997 Morcrette et al., 2001	Mlawer and Clough, 1997

Table 2: Results from 13-month simulations at $T_L159L91$. Radiative fluxes at TOA are compared to CERES measurements, total cloud cover (TCC) to ISCCP D2 data, total column water vapour (TCWV) and liquid water (TCLW) to SSM/I data. TP is the total precipitation compared to GPCP or SSM/I data. The surface fluxes are compared to the Da Silva climatology.

	Annual	DJF	JJA
OLR	-239	-236	-242
Oper	-8.1 (12.7)	-6.1 (15.0)	-5.1 (12.8)
McRad	-3.2 (7.9)	-1.1 (10.1)	-0.6 (10.5)
ASW	244	251	238
Oper	-10.0 (17.5)	-15.6 (23.9)	-9.2 (19.7)
McRad	-5.8 (14.2)	-11.4 (20.5)	-5.3 (18.6)
LWCF	27.3	26.8	26.1
Oper	-9.6 (13.6)	-10.4 (16.5)	-8.3 (14.1)
McRad	-4.0 (7.9)	-4.8 (10.3)	-3.0 (9.7)
SWCF	-48.7	-52.8	-45.1
Oper	-5.2 (15.4)	-4.1 (18.6)	-6.3 (18.2)
McRad	-0.2 (12.9)	0.5 (17.0)	-1.3 (17.3)
TCWV	29.0	27.7	29.3
Ope1	-2.10 (3.65)	-2.27 (4.29)	-1.73 (3.69)
McRad	-1.67 (3.13)	-1.80 (3.63)	-1.25 (3.32)
TCC	62.2	62.9	61.4
Oper	-6.0 (10.3)	-5.7 (12.3)	-5.4 (11.8)
McRad	-5.3 (9.5)	-4.9 (11.2)	-4.7 (11.4)
TCLW	82.2	80.4	84.3
Oper	1.67 (22.1)	3.13 (33.4)	-1.11 (30.6)
McRad	0.86 (22.4)	2.05 (32.8)	-1.21 (30.8)
TP gpcp	2.61	2.58	2.63
Oper	0.45 (1.39)	0.42 (1.88)	0.43 (1.75)
McRad	0.40 (1.21)	0.37 (1.60)	0.41 (1.72)
TP ssmi	3.80	3.57	3.66
Oper	0.67 (2.45)	0.57 (3.56)	0.44 (3.90)
McRad	0.50 (2.23)	0.38 (3.32)	0.35 (3.81)
SSR ocn	155.2	163.7	143.7
Oper	8.4	15.1	0.3
McRad	15.6	21.9	7.4
STR ocn	-51.8	-52.5	-50.4
Oper	0.6	1.0	1.3
McRad	-0.1	0.3	0.6
SSH ocn	-11.0	-13.7	-9.0
Oper	-4.7	-3.0	-5.9
McRad	-3.5	-2.0	-4.9
SLH ocn	-96.5	-100.2	-94.2
Oper	-10.5	-7.7	-11.1
McRad	-7.2	-4.5	-7.9
SNET ocn	-2.1	-0.9	-7.9
Oper	-8.1	3.6	-17.3
McRad	2.8	14.0	-6.8

Table 3: Results from 13-month simulations at $T_L 159 L91$ with different cloud configurations. G21 is the McRad model with generalized overlap of cloud layers with a decorrelation length for cloud cover DLCC=2 km and a decorrelation length for cloud water DLCW=1 km, G42 is with DLCC=4 km and DLCW=2 km, G51 with DLCC=5 km and DLCW=1 km. MR is the McRad model with maximum-random overlap of homogeneous clouds. All quantities are annual means. Radiative fluxes at TOA are compared to CERES measurements, total cloud cover (TCC) to ISCCP D2 data, total column water vapour (TCWV) and liquid water (TCLW) to SSM/I data. TP is the total precipitation compared to GPCP or over ocean to SSM/I data. The surface fluxes are compared to the Da Silva climatology.

	Observation	G21	G42	G51	MR
OLR	-239	-2.7 (7.8)	-4.3 (8.1)	-3.9 (7.8)	0.02 (8.3)
ASW	244	-5.9 (14.6)	-1.8 (12.5)	-1.9 (12.3)	-13.1 (19.5)
LWCF	27.3	-2.6 (6.9)	-4.0 (7.3)	-3.6 (7.0)	0.03 (7.5)
SWCF	-48.7	-0.2 (13.4)	3.8 (12.6)	-3.7 (12.4)	-7.5 (17.2)
TCWV	29.0	-1.38 (3.06)	-1.43 (3.03)	-1.40 (3.02)	-1.18 (2.92)
TCC	62.2	-1.04 (11.1)	-1.14 (11.0)	-1.00 (10.7)	-0.12 (10.9)
TCLW	82.2	-7.44 (22.7)	-7.45 (22.8)	-7.31 (22.7)	-5.37 (22.2)
TP gpcp	2.61	0.30 (1.17)	0.31 (1.15)	0.30 (1.14)	0.29 (1.19)
TP ssmi	3.80	0.31 (2.16)	0.30 (2.14)	0.26 (2.10)	0.31 (2.23)
SSR ocn	155.2	15.9	20.1	19.9	7.3
STR ocn	-51.8	-3.6	-5.0	-4.9	-0.5
SSH ocn	-11.0	-1.6	-1.6	-1.5	-1.5
SLH ocn	-96.5	-4.2	-4.1	-3.5	-4.1
SNET ocn	-2.1	4.5	7.4	7.9	-0.8

Table 4: Impact of the McRad radiation package on the timing of the ECMWF model forecasts at different horizontal resolutions. All results are for a model with 91 vertical levels. *Dyn* is the resolution for the dynamics, *Rad* that for the radiation. *Freq* is the frequency (hour) for calling the full radiation scheme, *%Rad* is the fraction of computer time taken by the radiative transfer calculations. *Ratio* is the increase factor brought by McRad over the total computer cost of the previous operational configuration (ref31R1).

	Dyn	Rad	Freq	%Rad	Ratio
ref31R1	799	399	1	7.3	1.000
McRad	799	399	1	26.8	1.277
	799	319	1	19.5	1.201
	799	255	1	14.0	1.148
	799	159	1	7.0	1.075
	799	95	1	3.6	1.038
	McRad	799	399	3	10.8
	799	319	3	8.2	1.090
	799	255	3	5.7	1.060
ref31R1	399	159	3	4.8	1.000
McRad	399	159	3	18.0	1.183
ref31R1	255	95	3	6.2	1.000
McRad	255	95	3	22.6	1.221
ref31R1	159	63	3	8.5	1.000
McRad	159	63	3	29.5	1.319
ref31R1	95	95	3	27.2	1.000
McRad	95	95	3	69.9	1.712
	95	63	3	52.8	1.539

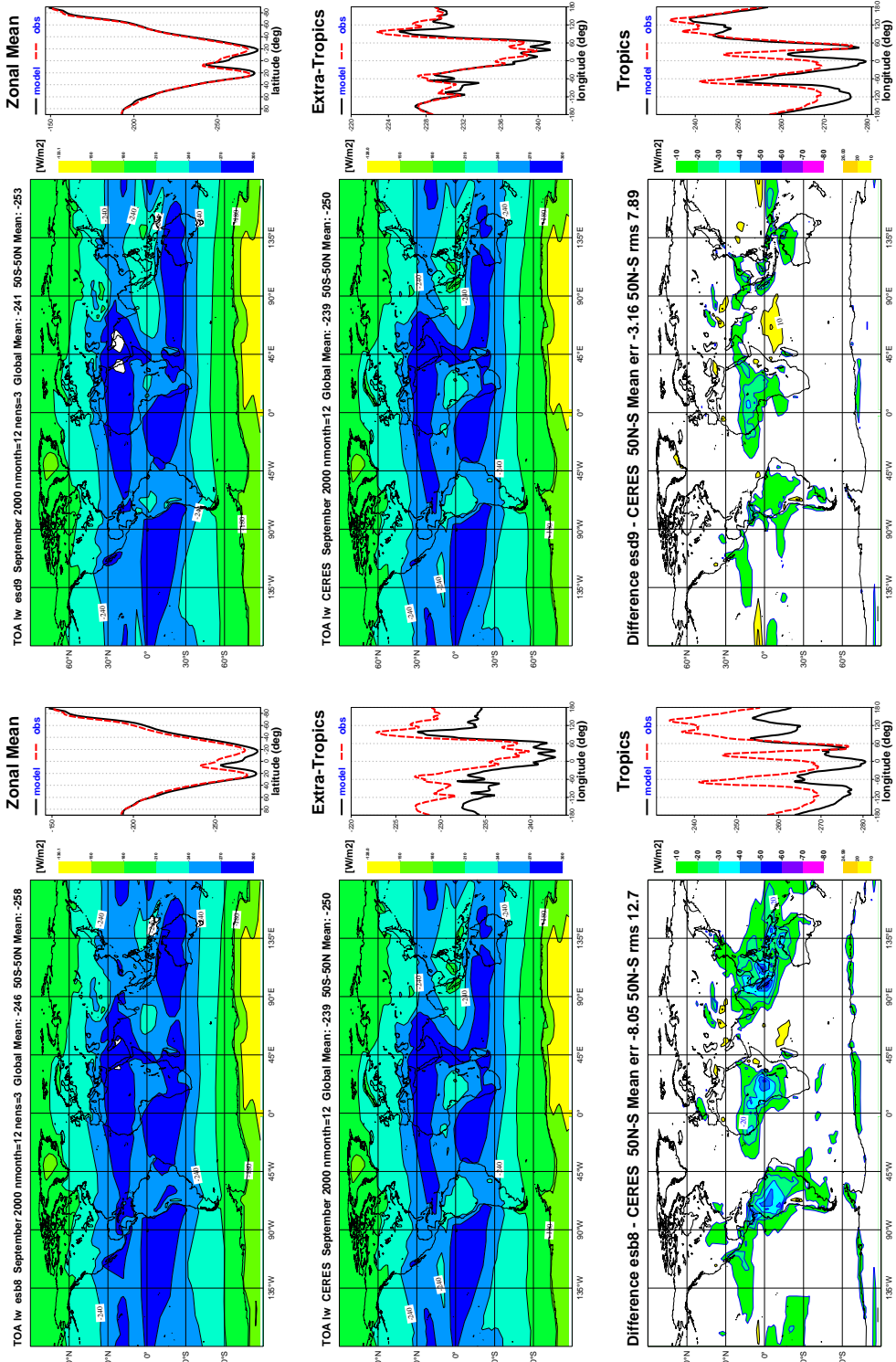


Figure 1: The outgoing longwave radiation at the top of the atmosphere (in Wm^{-2}). Top figures are the ECMWF model simulations (left: operational, right: McRad), middle ones are the CERES observations, bottom ones are the differences between simulations and observations.

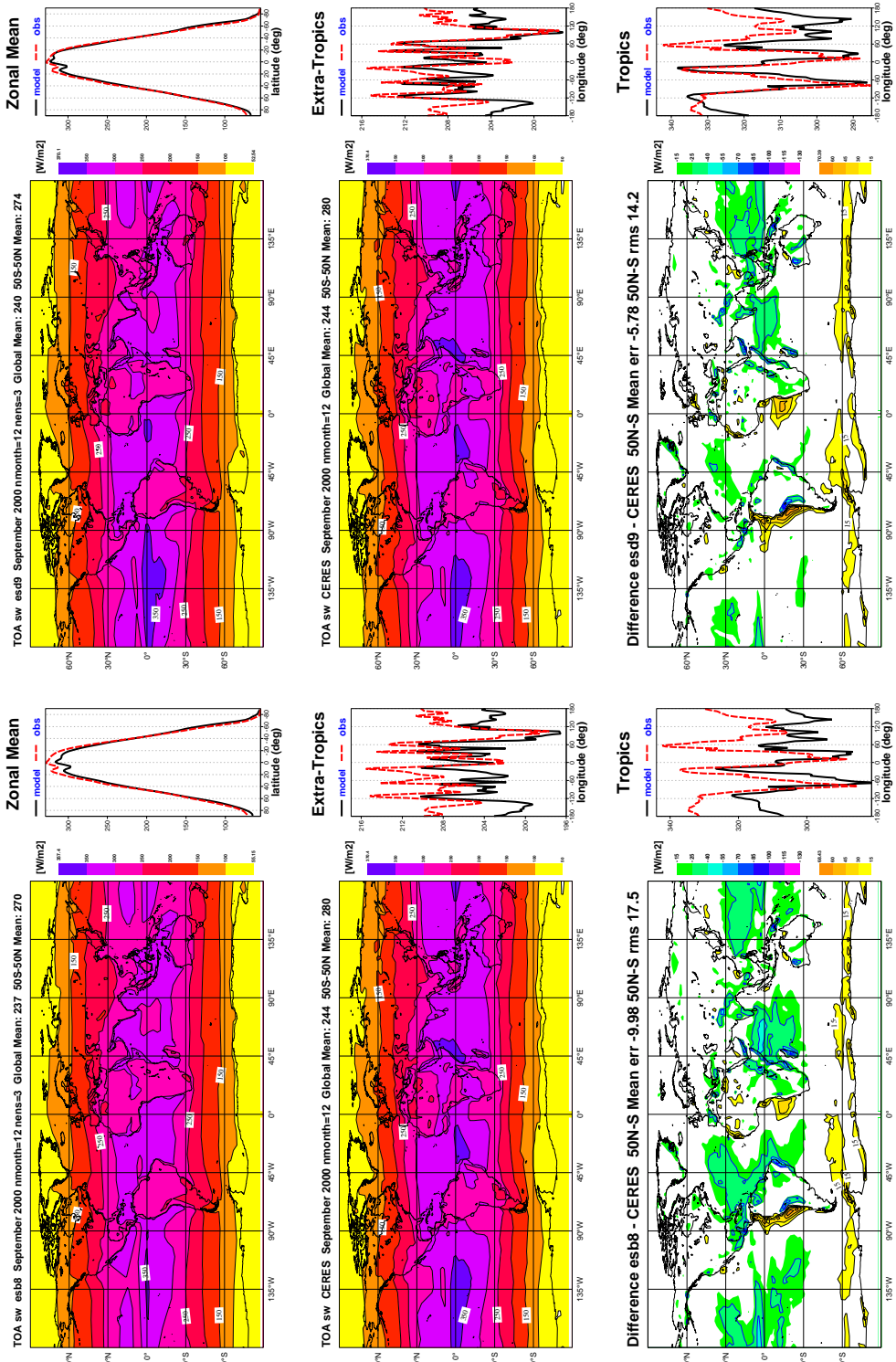


Figure 2: The absorbed shortwave radiation in the atmosphere (in Wm^{-2}). Top figures are the ECMWF model simulations (left: operational, right: McRad radiation), middle ones are the CERES observations, bottom ones are the differences between simulations and observations.

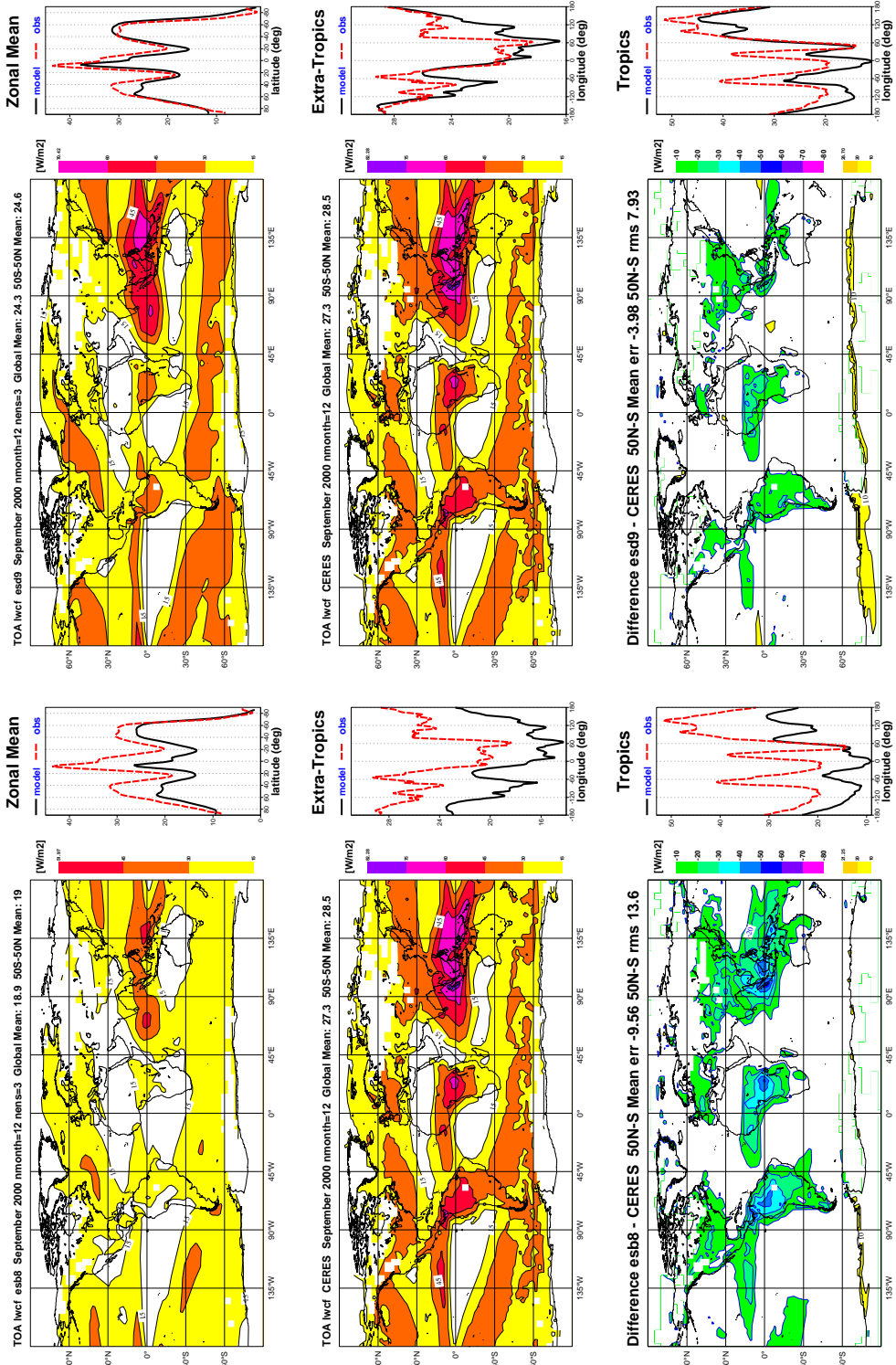


Figure 3: The longwave cloud forcing (in Wm^{-2}). Top figures are the ECMWF model simulations (left: operational, right: McRad), middle ones are the CERES observations, bottom ones are the differences between simulations and observations.

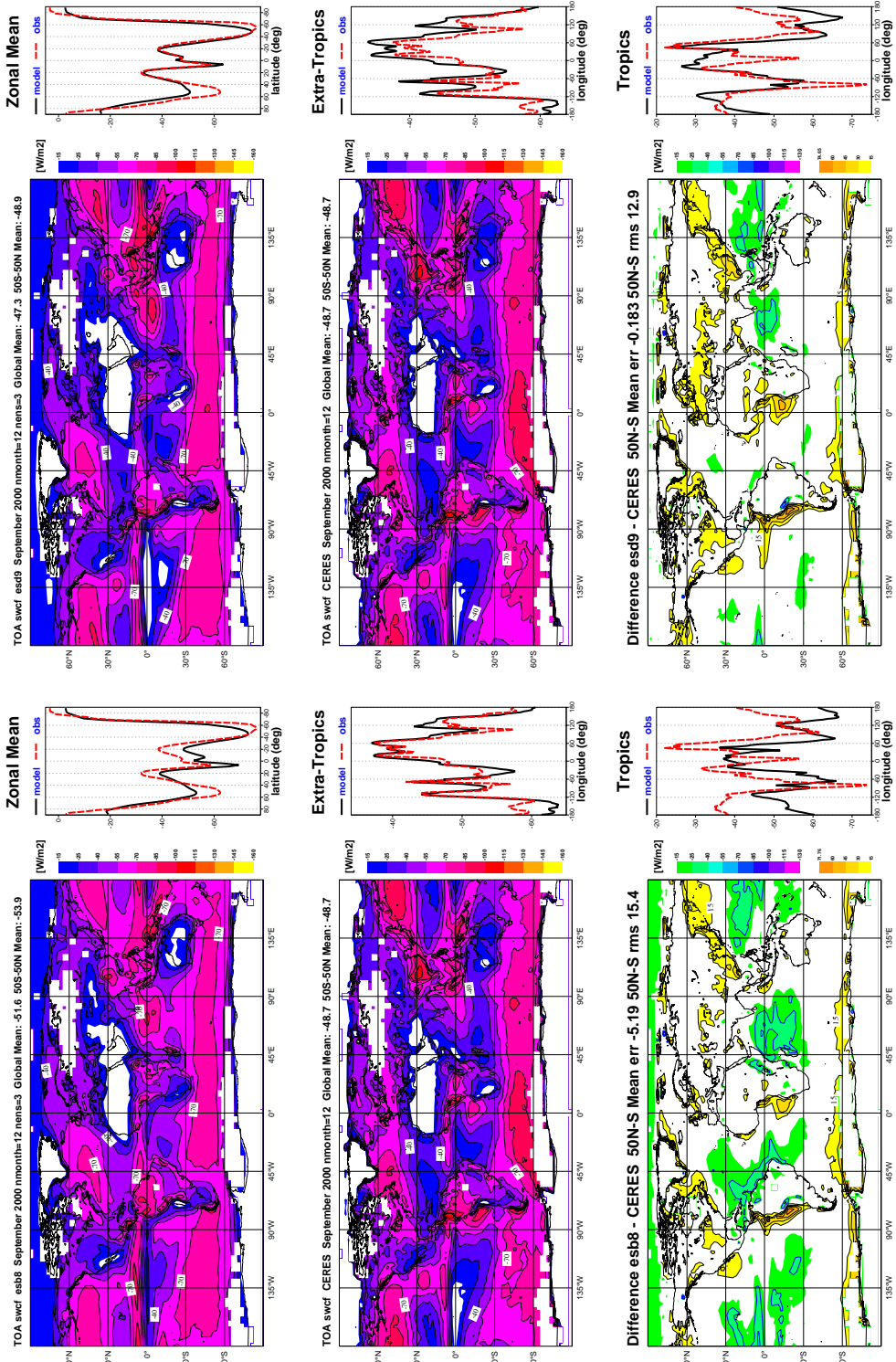


Figure 4: The shortwave cloud forcing (in Wm^{-2}). Top figures are the ECMWF model simulations (left: operational, right: McRad), middle ones are the CERES observations, bottom ones are the differences between simulations and observations.

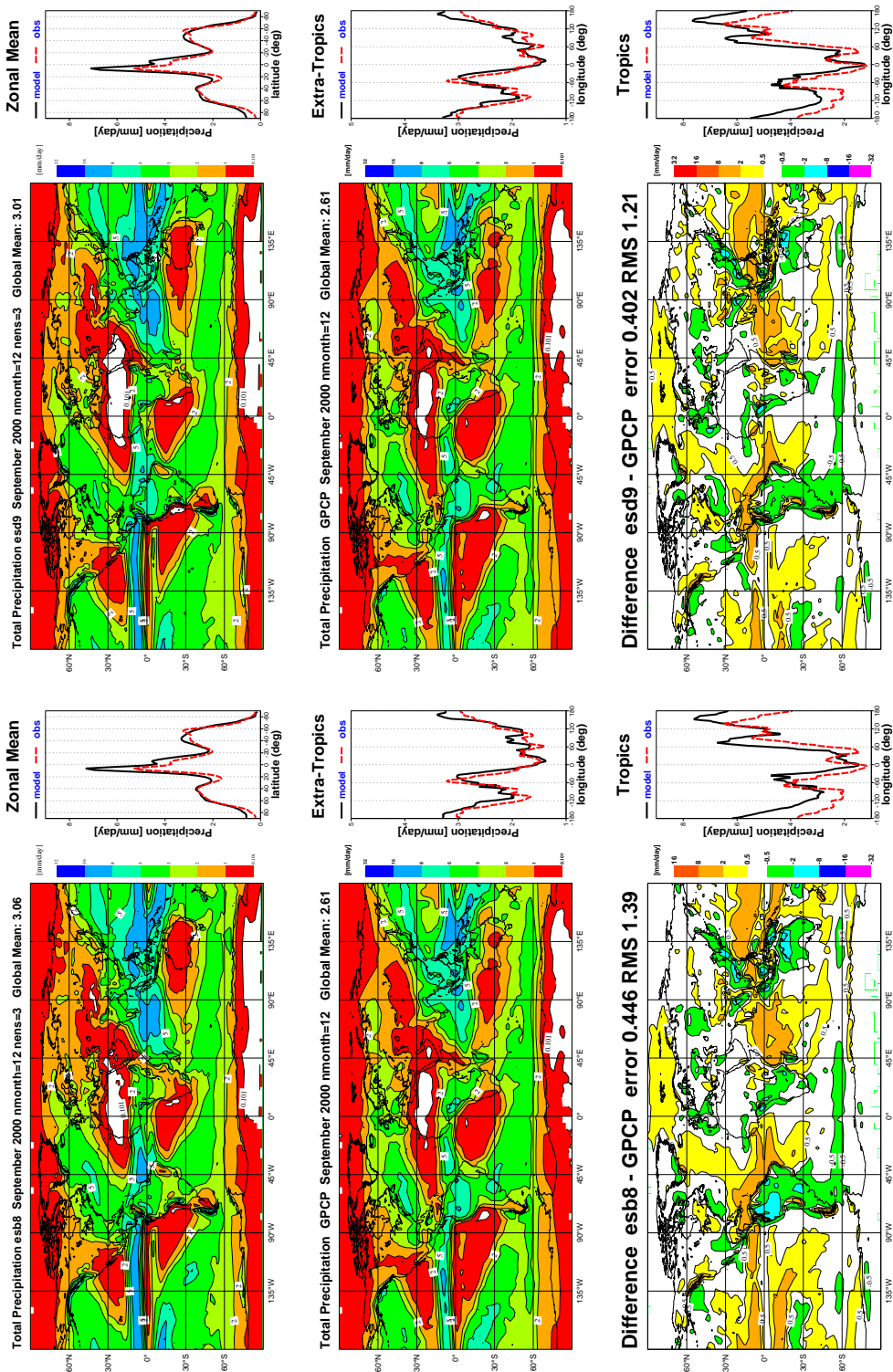


Figure 5: The total precipitation (in mm day^{-1}). Top figures are the ECMWF model simulations (left: operational, right: McRad), middle ones are the GPCP observations, bottom ones are the differences between simulations and observations.

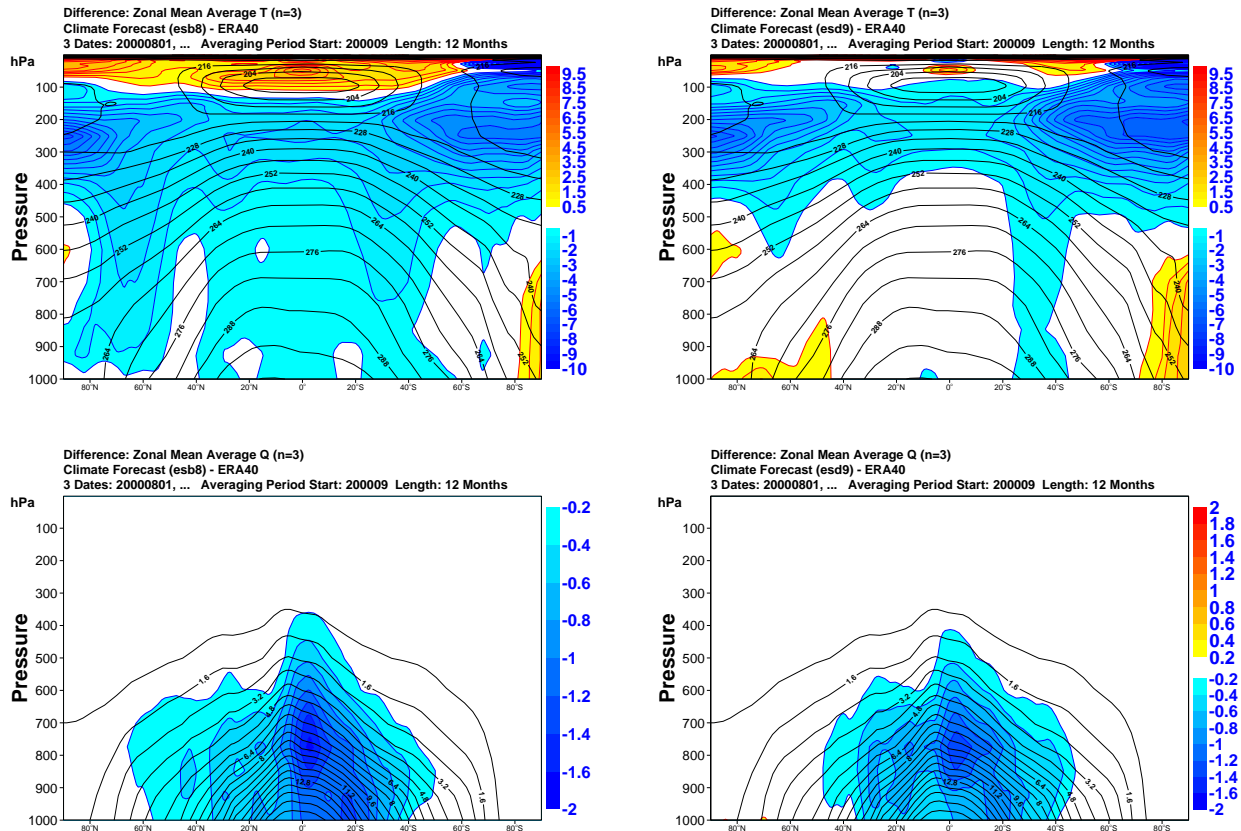


Figure 6: The difference with ERA40 analysis for temperature (top panels, in K) and humidity (bottom panels, in kg kg^{-1}). Left column is for the operational model; right one for the model with McRad.

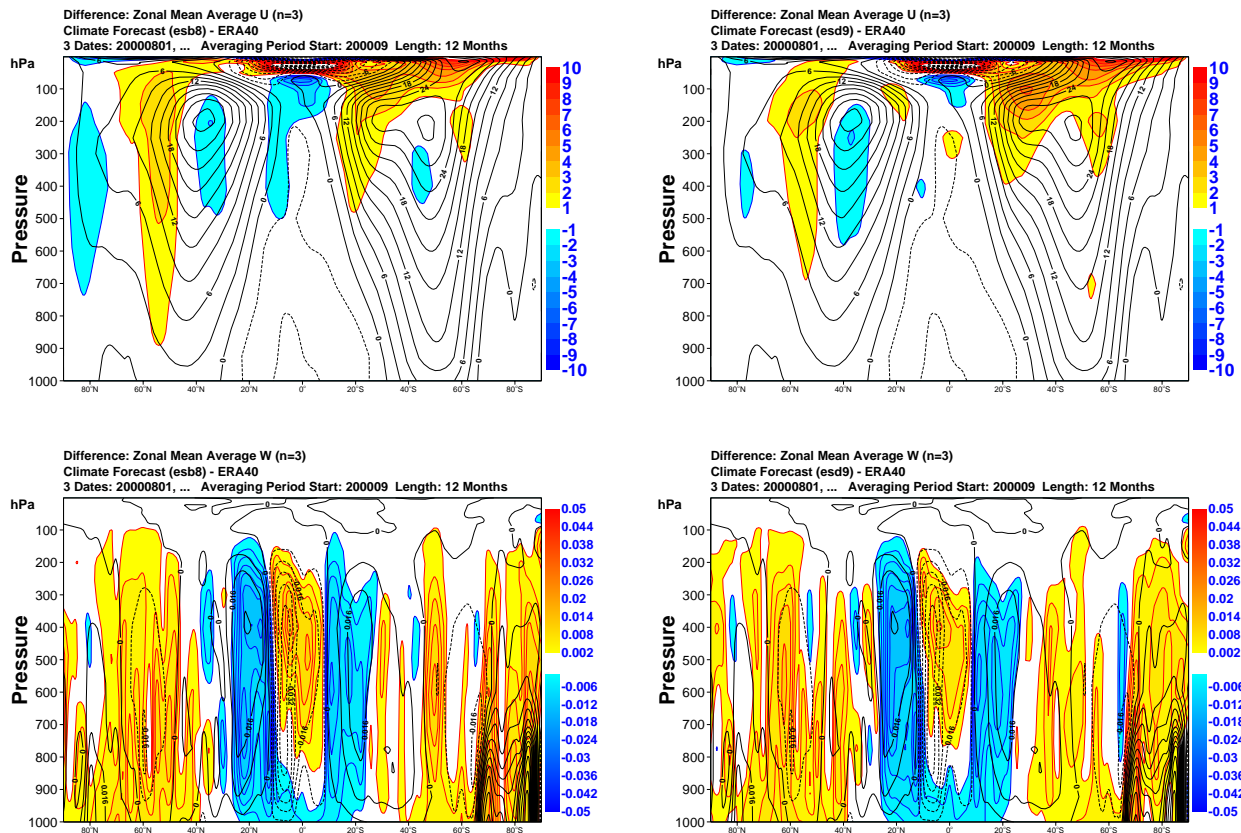


Figure 7: The difference with ERA40 analysis for zonal wind (top panels, in $m s^{-1}$) and vertical velocity (bottom panels, in $Pa s^{-1}$). Left column is for the operational model; right one for the model with McRad.

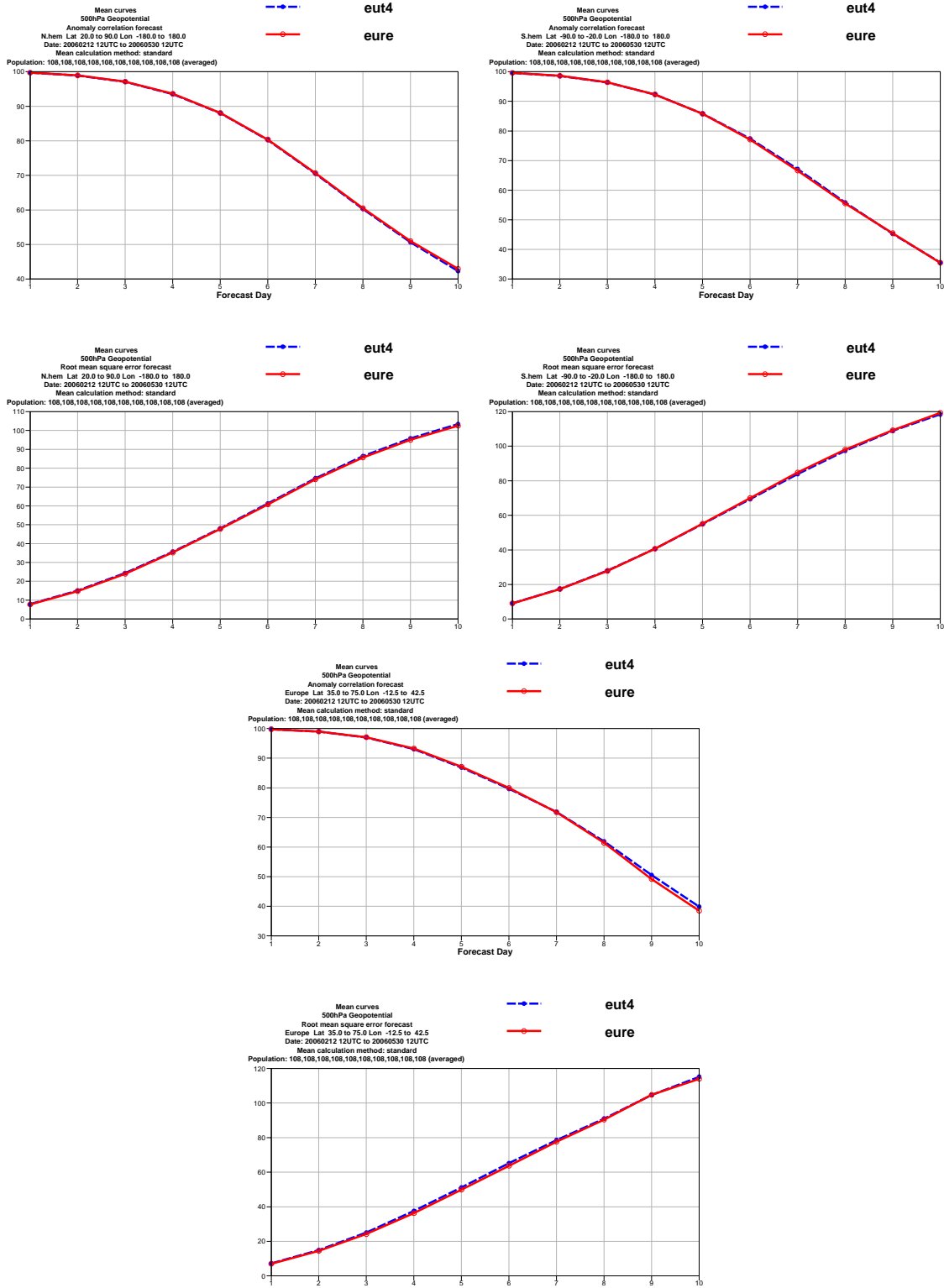


Figure 8: The anomaly correlation of the geopotential at 500hPa (Z500) (top panels) and the root mean square error on Z500 (bottom panel) over the Northern hemisphere (upper left), Southern hemisphere (upper right), and Europe (lower panels) for the reference (blue) and McRad (red) models for a set of $T_L319L91$ 10-day forecasts, started every 24 hours from 2006021212 to 2006053012.

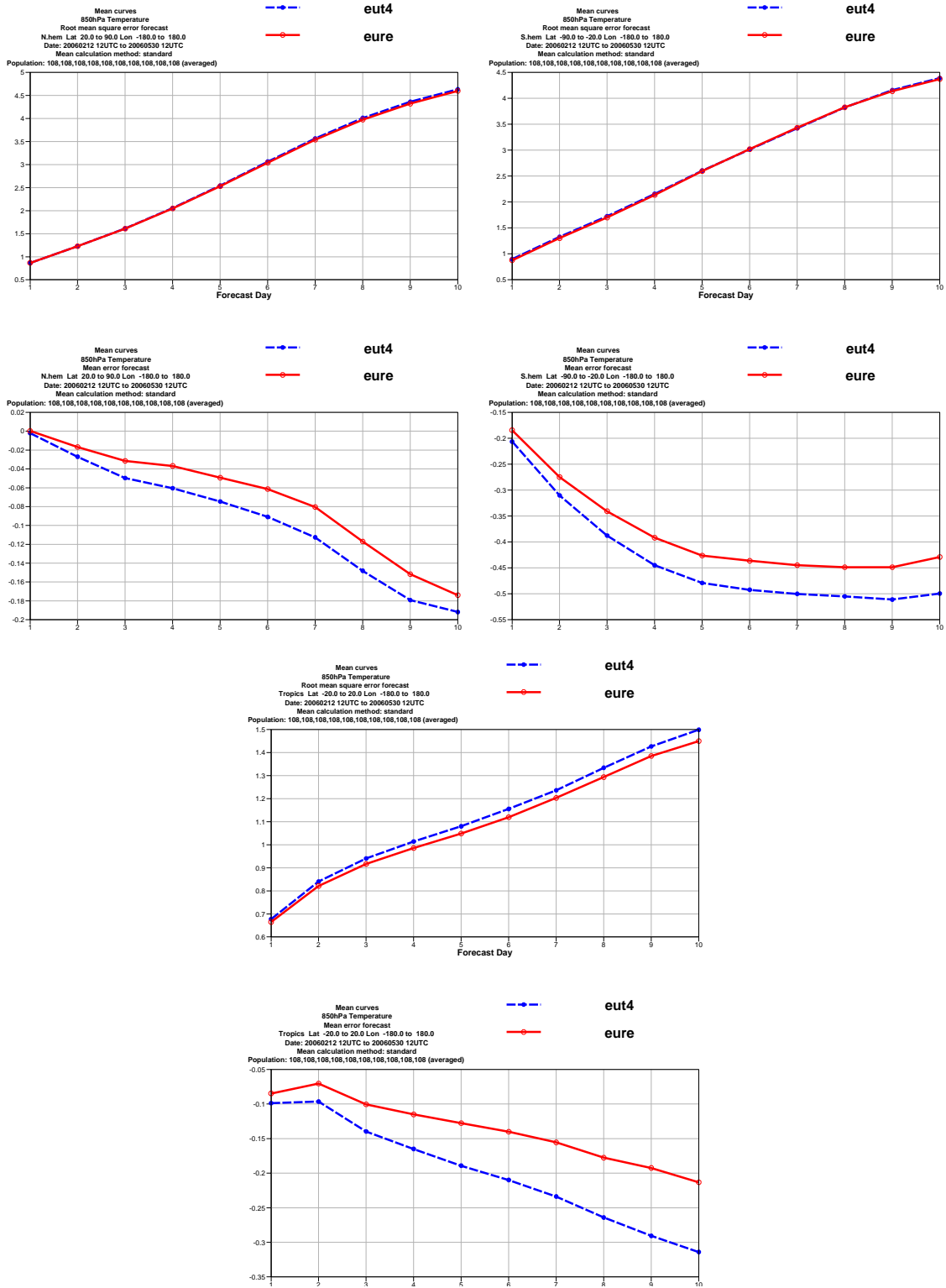


Figure 9: The root mean square error (top) and mean error (bottom) of the temperature at 850 hPa. Northern hemisphere is top left, Southern hemisphere is top right, Tropics (20°N - 20°S) is bottom central. Reference is in blue and McRad is in red. for a set of 10-day forecasts at T_319L91 10-day, started every 24 hours from 2006021212 to 2006053012.

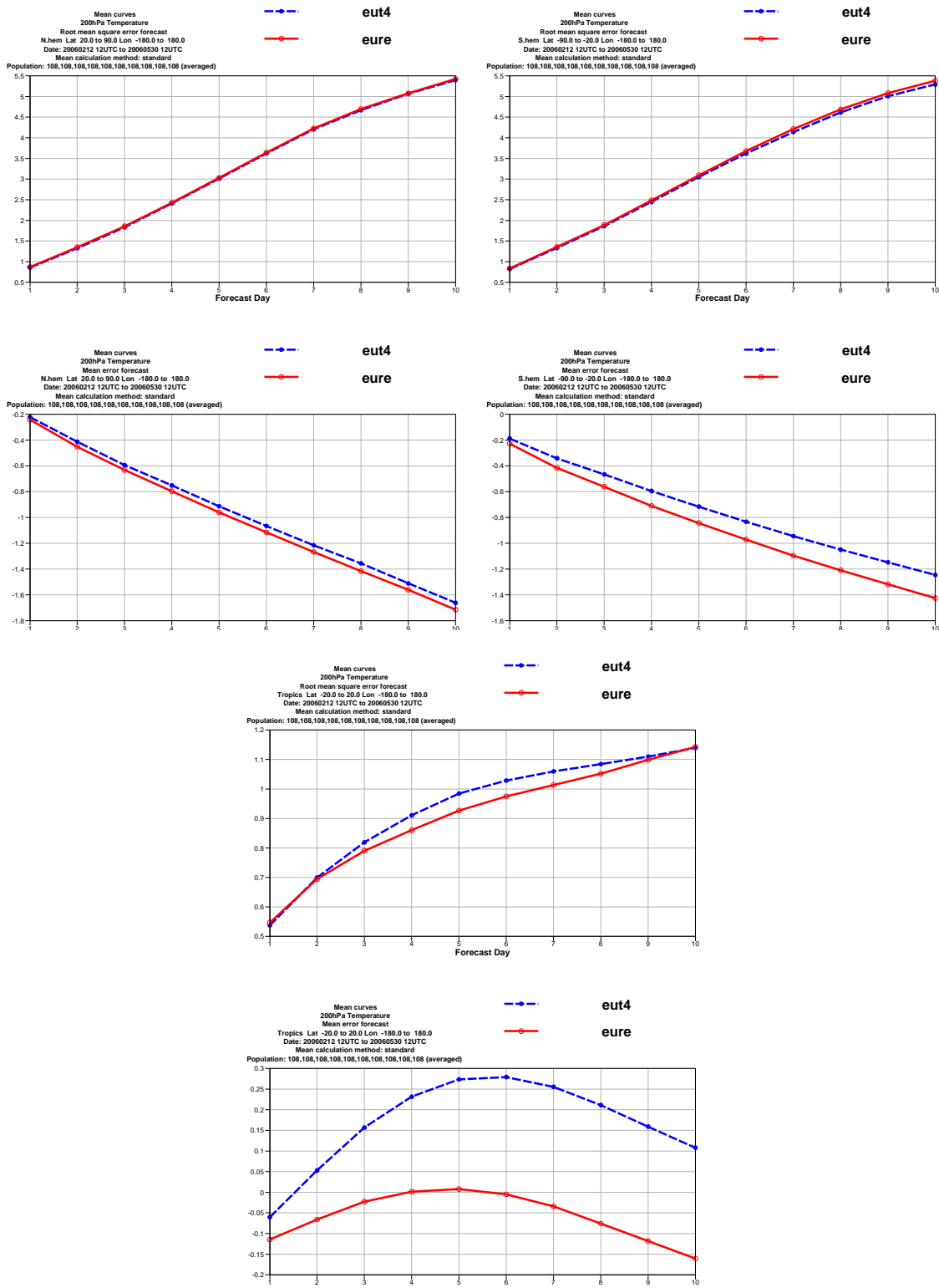


Figure 10: As in Fig9, but for the temperature at 200 hPa.

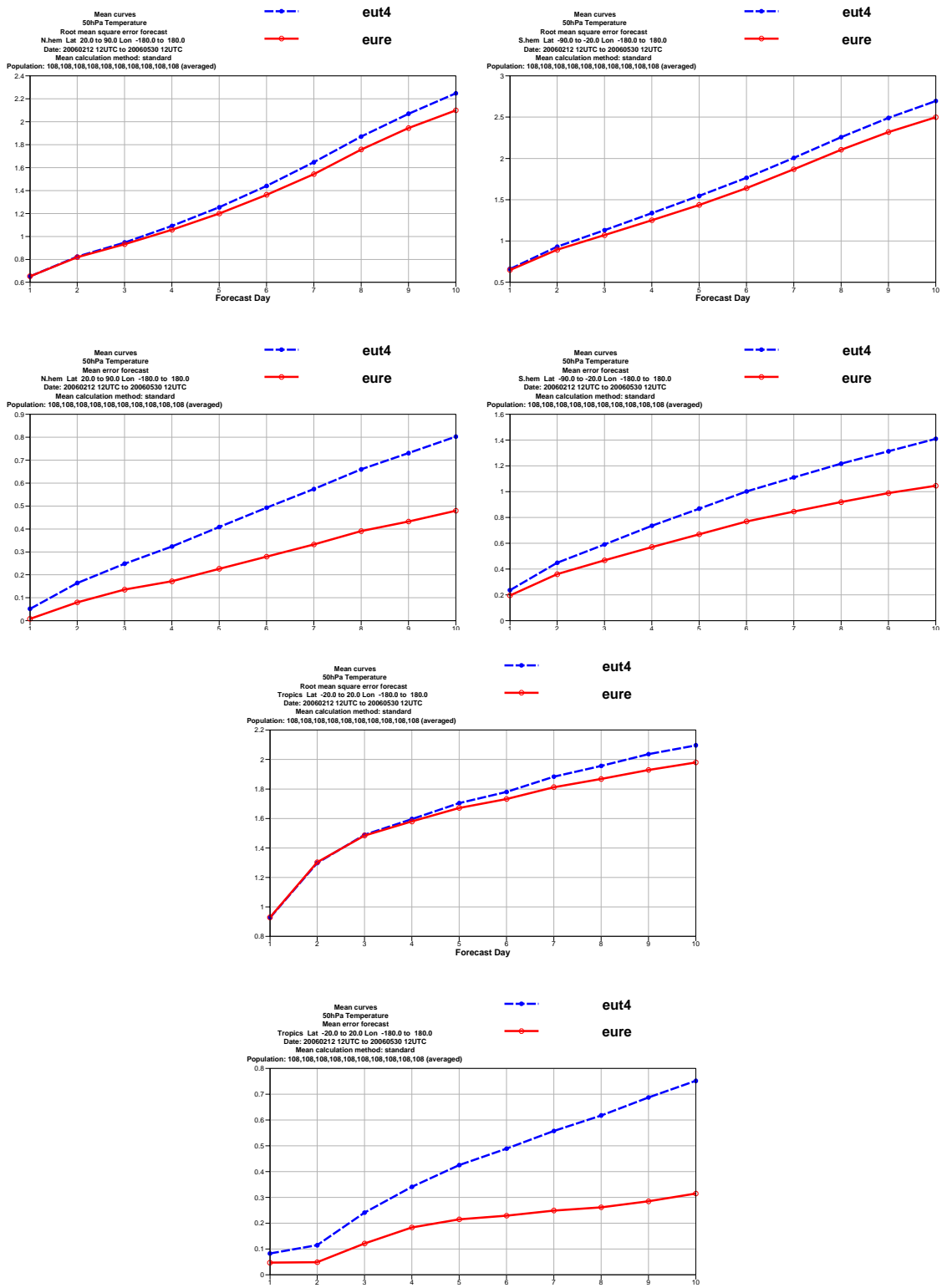


Figure 11: As in Fig9, but for the temperature at 50 hPa.

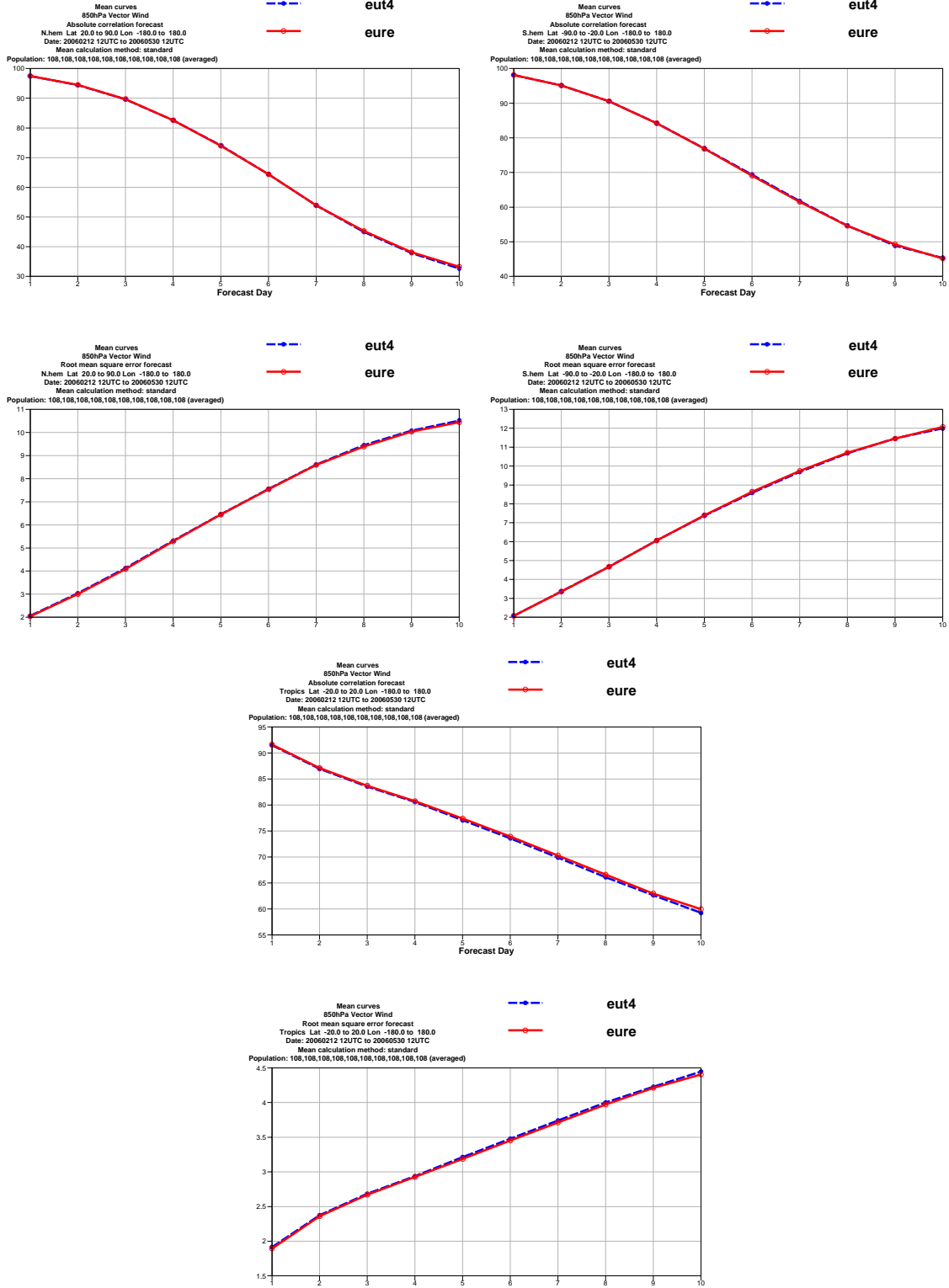


Figure 12: The absolute correlation (top) and root mean square error (bottom) of the wind at 850 hPa. Northern hemisphere is top left, Southern hemisphere is top right, Tropics (20°N - 20°S) is bottom central. Reference is in blue and McRad is in red. for a set of 10-day forecasts at $T_L319L91$ 10-day, started every 24 hours from 2006021212 to 2006053012.

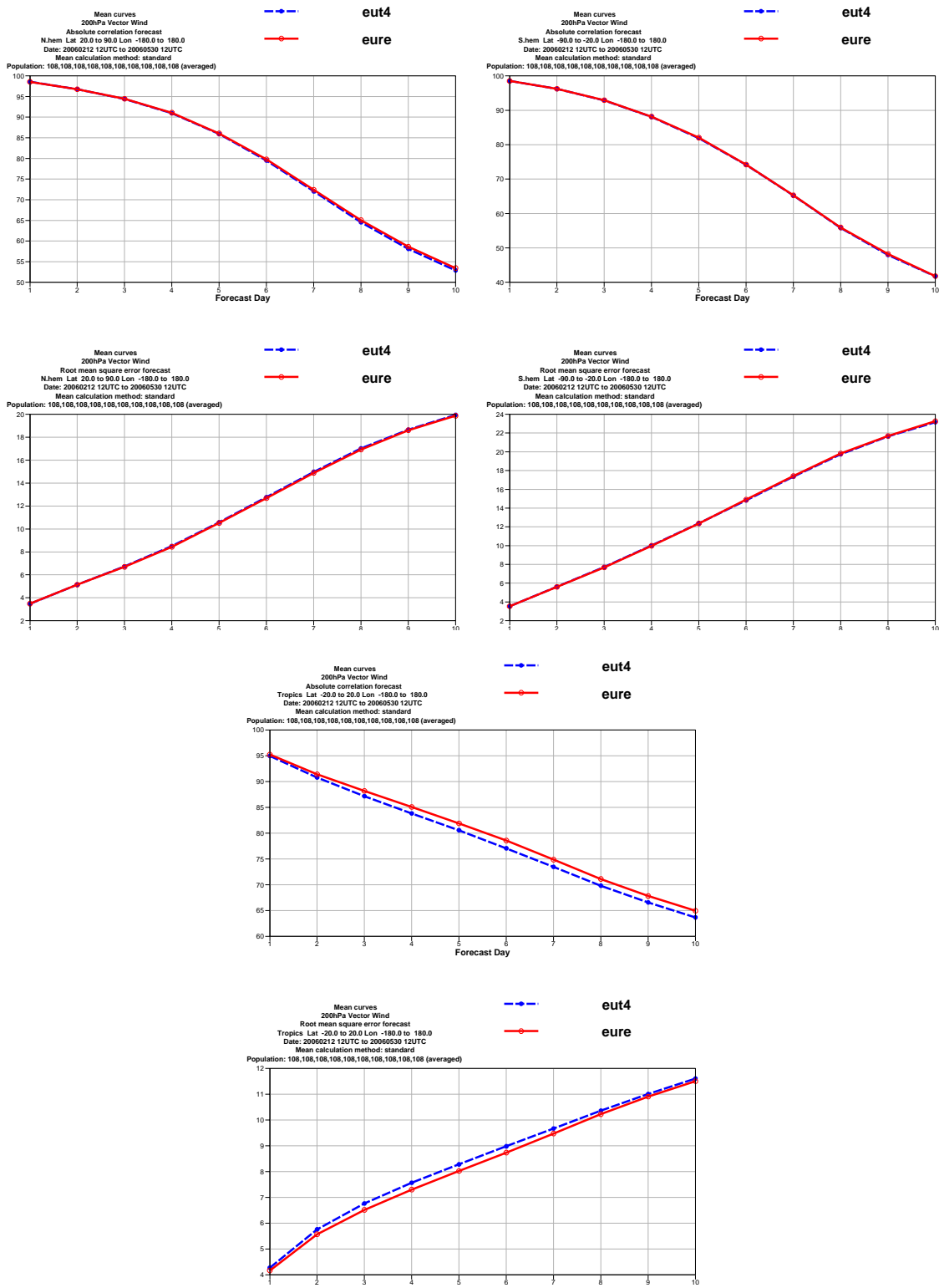


Figure 13: As in Fig12, but for the wind at 200 hPa.

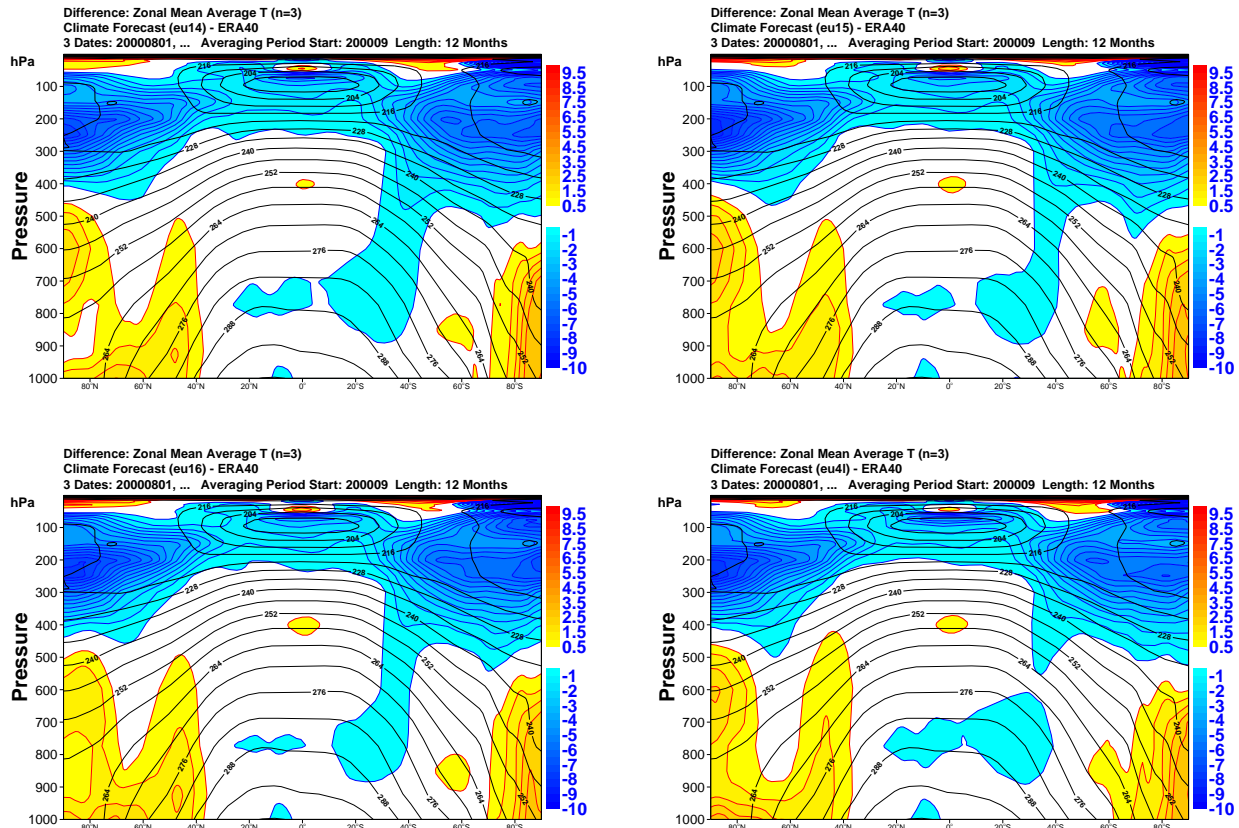


Figure 14: The difference with ERA40 analysis for temperature (top panels, in K). Top left is the McRad model with generalized overlap of cloud layers with a decorrelation length for cloud cover $DLCC=2$ km and and a decorrelation length for cloud water $DLCW=1$ km, top right with $DLCC=4$ km and $DLCW=2$ km, bottom left with $DLCC=5$ km and $DLCW=1$ km. Bottom right is the McRad model with maximum-random overlap of homogeneous clouds.